Subsurface Near-Field Scanning Tomography

K. P. Gaikovich

Institute for Physics of Microstructures of RAS, GSP-105, Nizhniy Novgorod, Russia, 603950
(Received 2 June 2006; published 1 May 2007)

The scanning tomography method is developed for electromagnetic sounding of a 3D structure of an inhomogeneous dielectric half-space. It is shown that known methods of physical diagnostics are suitable for this tomography with the depth of analysis from nanometers at optical frequencies up to several kilometers at ultralow frequencies. The areas of application include nanophysics, biological and medical diagnostics, subsurface remote sensing in geophysics and geology, etc. This approach is realized in the microwave scanning tomography of living tissues where a subwavelength resolution is achieved.

By now, various kinds of computer tomography are widely in use. The general approach to this problem is based on Radon's transform [1] and methods of ill-posed problem solutions [2]. The method of the near-field scanning tomography (NST), proposed in this Letter, uses data of the 2D scanning of a probe along the plane interface of an absorbing dielectric half-space ($z \leq 0$) with a 3D inhomogeneous region dependent on a parameter of the received signal that determines the effective depth of its formation (the depth-of-formation parameter).

Similar mathematical ideas have been realized in the near-field optics in [3–8] to obtain the 3D structure of dielectric susceptibility of samples in the free space that are exposed into single evanescent plane waves launched at the total internal reflection of rays in prisms or semi-cylinders. These resources cover a variety of measurement modalities including total-internal-reflection tomography based on scattered field measurements and scanning near-field optical microscopy (SNOM) probe measurements of the scattered field intensity in the collection mode. An experimental demonstration of this approach is given for the case of 2D samples in [7].

It should be mentioned that when scanning a half-space from an upper half-space with a higher refractivity, approaches developed in [3–8] can also be used in NST. But in the case of NST that uses measurements of a dielectric half-space from the vacuum, it is impossible to launch single evanescent waves because of the absence of the total internal reflection. To overcome this problem, the property of a small-aperture source (positioned in the near-field zone above the surface) to generate a spectrum of evanescent waves into a half-space is used in the proposed tomography based on SNOM measurements in the illumination mode. But, unlike the SNOM collection mode considered in [3–8], the kernel of the corresponding one-dimensional Fredholm integral equation depends on the source (probe) parameters such as its sizes and the altitude above the surface, and these parameters can be used as the depth-of-formation parameter instead of wave vector components in [3–8].

This dependence of the effective depth of formation of the received signal on the small-aperture probe size and on its altitude above the interface has been discovered recently in the thermal radio emission of an absorbing dielectric medium [9,10], and this dependence is used here in the microwave tomography of the subsurface temperature and permittivity. For the tomography of an absorbing half-space with the frequency-dependent skin depth, the frequency can also be considered as the depth-of-formation parameter.

It is shown here that various known methods of physical diagnostics (SNOM, radiometry, insertion impedance diagnostics, magnetotelluric sounding) can be transformed into NST methods, and, as the main result, the method of microwave NST is demonstrated to retrieve the 3D dielectric structure of living tissues with a subwavelength resolution.

Theory.—Let us consider a scattering region with the complex permittivity $\varepsilon(\mathbf{r}, \omega) = \varepsilon_0(\omega) + \varepsilon_1(\mathbf{r}, \omega)$ (ω is the cyclic frequency), that is embedded in a half-space $z \leq 0$ with $\varepsilon = \varepsilon_0(\omega)$. In the upper half-space $\varepsilon = 1$ is assumed, but all the results are valid for any other constant value of permittivity. For the time dependence $\exp(i\omega t)$, the reference (unperturbed) field $\mathbf{E_0}(\mathbf{r})$ is determined by the known Green tensor (that includes near-field components):

$$\mathbf{E}_0(\mathbf{r}) = \frac{1}{i\omega} \int_V \overleftrightarrow{\mathbf{G}}(\mathbf{r} - \mathbf{r'})\mathbf{j^p}(\mathbf{r'})d\mathbf{r'}, \qquad (1)$$

where $\mathbf{j^p}(\mathbf{r})$ is the current distribution in the source. Using the plane waves' decomposition of (1), it is possible to obtain the refracted field $\mathbf{E_0}(\mathbf{r})$ at $z \leq 0$. In the presence of the scattering region, the electric field $\mathbf{E}(\mathbf{r})$ is obtained in frameworks of perturbation theory from

$$\mathbf{E}(\mathbf{r}) = \mathbf{E_0}(\mathbf{r}) + \frac{1}{4\pi\varepsilon_0} \int_V \overleftrightarrow{\mathbf{R}}(\mathbf{r}, \mathbf{r'})\mathbf{E_0}(\mathbf{r'})d\mathbf{r'}. \qquad (2)$$

The resolvent **R** is determined by known Neumann series using ε_1 and the proper Green function. Equations (1) and (2) solve the direct problem of electrodynamics. An effective approach to this direct problem, based on the solution

of a Dyson's equation for the resolvent, was developed in
[11]. Unfortunately, the solution of the inverse problem for
the nonlinear integral equation (2) with a 6D kernel is a
very complicated problem. For this reason, in problems
where scattered fields are in use, our consideration is based
on the Born approximation ($\varepsilon_1(\vec{r}) \ll \varepsilon_0$, where $\mathbf{E}(\mathbf{r}) \approx$
$\mathbf{E_0}(\mathbf{r}) + \mathbf{E_1}(\mathbf{r})$ and scattered fields' components are deter-
mined as

$$\mathbf{E}_1(\mathbf{r}) = \frac{1}{4\pi\varepsilon_0} \int_V \varepsilon_1(\mathbf{r}')\overleftrightarrow{\mathbf{G}}_\mathbf{E}(\mathbf{r} - \mathbf{r}')\mathbf{E_0}(\mathbf{r}')d\mathbf{r}',$$

$$\mathbf{H}_1(\mathbf{r}) = \frac{i\omega}{4\pi c} \int_V \varepsilon_1(\mathbf{r}')\overleftrightarrow{\mathbf{G}}_\mathbf{H}(\mathbf{r} - \mathbf{r}')\mathbf{E_0}(\mathbf{r}')d\mathbf{r}'. \quad (3)$$

$$\mathbf{E}_\mathbf{1}(\kappa_x, \kappa_y, z) = \frac{\pi}{\varepsilon_0} \int_{-\infty}^0 \varepsilon_1(\kappa_x - k_x, \kappa_y - k_y, z')\overleftrightarrow{\mathbf{G}}_\mathbf{E}(\kappa_x, \kappa_y, z, z')\mathbf{E_0} \exp(\pm i\sqrt{k^2 - k_\perp^2}\, z')dz', \quad (4)$$

where $k^2 = (\omega/c)^2\varepsilon_0$, the sign in exp() should correspond
to extinction. One can see in (4) the effect of the shift of the
permittivity spectrum relative to the field spectrum that
makes it possible to realize the subwavelength resolution at
far-field measurements using in the sounding single eva-
nescent plane waves (at the value of $k_\perp^2 = k_x^2 + k_y^2 > |k|^2$)
just like in methods found in [3–8].

There is also the second possibility of NST that uses a
near-field source itself in 2D lateral scanning, as, for
example, in the SNOM illumination mode. In such cases,
it appears possible to express field parameters in the form
of 2D convolution equations over lateral coordinates of the
probe and to use these equations in NST.

Low frequency NST tomography.—The simplest appli-
cation of NST can be based on the ultralow frequency
electromagnetic sounding [9,12] of the earth crust up to
several kilometers in depth. At low frequencies $\varepsilon = \varepsilon' -$
$i\varepsilon'' \approx -i4\pi\sigma/\omega$, where σ is conductivity, and the ap-
proximation of Leontovich is valid. When, for example,
2D measurements of the y component of the magnetic field
are available at the surface level ($z = 0$), one has from (3):

$$H_{1y}(\kappa_x, \kappa_y, \omega, 0) = H_{0y}\frac{(1 + i)\omega\delta}{4c^2} \int_{-\infty}^0 \sigma_1(\kappa_x, \kappa_y, z')$$
$$\times \exp\left(\frac{z'}{\delta} + i\frac{z'}{\delta}\right)$$
$$\times \exp[\pm i\sqrt{k^2 - \kappa_\perp^2}\, z']dz', \quad (5)$$

where $\delta = c/\sqrt{2\pi\omega\sigma_0}$ is the skin depth, and σ_1 is the
lateral spectrum of conductivity variations.

To retrieve depth profiles $\sigma_1(\kappa_x, \kappa_y, z)$ from the one-
dimensional Fredholm integral equation of the first kind
(5) with the frequency as the depth-of-formation parame-
ter, the mathematically consistent algorithm is developed
here that is based on Tikhonov's method of generalized
discrepancy [12]. The regularization parameter determined
by the integral error of lateral spectrum is derived from the
known integral error of the measured signal using

Using the plane waves' decomposition in (3) at $z \leq 0$, it
is possible to obtain scattered fields in the upper half-space
where they can be measured. At the fixed position of the
source of unperturbed field, Eqs. (3) are not, in general,
simple convolution equations over lateral coordinates of a
receiver, but they are systems of 3 convolution equations
(because $\overleftrightarrow{\mathbf{G}}$ is a tensor), so it is not easy to use scattered
fields (or intensities) in the proposed NST. But there are
ways out. First, the reference field in a medium can be a
plane wave $\mathbf{E_0}(\mathbf{r}) = \mathbf{E_0}\exp(i\mathbf{k}\mathbf{r})$ that has no fixed source.
Using the known property of the Fourier transform of a
product with an exponent, one has from (3) the spectrum of
the scattered field:

Plansherel's theorem (the key point). Finally, the desired
3D structure of the conductivity $\sigma_1(x, y, z)$ is obtained by
2D inverse Fourier transform of the retrieved $\sigma_1(\kappa_x, \kappa_y, z)$.

NST tomography in SNOM.—The NST based on the
SNOM collection mode with the sample in a half-space
can be modified to the measurements scheme [5]. It is also
possible to develop NST methods based on SNOM in the
illumination mode, where a near-surface subwavelength
(electrically small) source is used for 2D scanning, and
measured parameters of scattered field can be expressed in
the form of a 2D convolution equation. Typically, the
received signal is collected in the far zone behind the
studied region, and it can be expressed as $S(\mathbf{r_1}) =$
$\iint c/8\pi\mathrm{Re}[\mathbf{E} \cdot \mathbf{H}^*]_z dx dy$, where $\mathbf{r_1}$ is the probe position.
The expression for variations of the signal at the probe
scanning $S_1(\mathbf{r_1}) \cong \iint c/16\pi[(E_{0x}H_{1y}^* - E_{0y}H_{1x}^* + E_{1x}H_{0y}^* -$
$E_{1y}H_{0x}^*) + \text{c.c.})dx dy$ appears to be a convolution equation
over lateral coordinates of the probe, so its 2D Fourier
transform leads to the one-dimensional integral expression.
This equation can be reduced to the Fredholm integral
equation of the first kind in two cases: when $\varepsilon_1 = \varepsilon_1'$ or
$\varepsilon_1 = -i\varepsilon_1''$. For example, if $\varepsilon_1 = \varepsilon_1'$,

$$S_1(k_x, k_y, z_1, D) = \int_{-\infty}^0 \varepsilon_1'(k_x, k_y, z')$$
$$\times K(j^p, k_x, k_y, \varepsilon_0, z_1, D, z')dz', \quad (6)$$

and (6) can be solved to obtain $\varepsilon_1'(x, y, z)$ just as σ_1 in
Eq. (5). The kernel K of (6) depends on depth-of-formation
parameters: a probe size parameter D and the probe alti-
tude z_1.

Microwave NST tomography.—Passive (radiometry)
microwave measurements have been in use in the one-
dimensional temperature sounding (profiling) in various
media (see [9]). From the general equation [9] for the
measured effective radio brightness, assuming $\varepsilon = \text{const}$
at $z \leq 0$, one obtains the exact expression for radio bright-
ness variations $T_{B1}(x, y, D)$:

$$T_{B1}(x_1, y_1, D) = \iint_{x,y} \int_{-\infty}^{0} T_1(x', y', z') \frac{|\mathbf{E_0}(x' - x_1, y' - y_1, z', z_1)|^2}{\iint_{x,y} \int_{-\infty}^{0} |\mathbf{E_0}(x' - x_1, y' - y_1, z', z_1)|^2 dx' dy' dz'} dx' dy' dz', \quad (7)$$

where $T_1(\mathbf{r})$ are temperature variations, $\mathbf{E}_0(\mathbf{r}' - \mathbf{r_1})$ is the field of the receiver antenna (attached to the point $\mathbf{r_1}$) when it works in the active mode, D is a depth-of-formation parameter (frequency, sizes of the antenna aperture, or its altitude z_1). At near-field measurements, plane resonant antennas [9,10] are in use that are matched to achieve near-zero reflection conditions. The master equation (exact) is obtained by 2D Fourier transform of (7)

$$T_{B1}(k_x, k_y, D) = \int_{-\infty}^{0} T_1(k_x, k_y, z') K(k_x, k_y, D, z',) dz' \quad (8)$$

and processed further in the same way as in the above-considered cases to obtain $T_1(x, y, z)$.

In the active (impedance) microwave sounding of media [9,13], variations of the signal reflected from resonant antennas are related to insertion impedance variations that are caused by variations of the subsurface permittivity. The variations R_1 of the reflection coefficient R can be measured, and, at the properly chosen frequency, they are proportional to variations of the antenna reactance [13]. Neglecting scattered fields and introducing the effective permittivity $\varepsilon_1^{\text{eff}} = (\Delta \varepsilon' / \Delta R) R_1$ as a product of the calibration constant and R_1, one obtains the desired expression:

$$\varepsilon_1^{\text{eff}}(x_1, y_1, D) = \iint_{x,y} \int_{-\infty}^{0} \varepsilon_1'(x', y', z') \frac{|\mathbf{E_0}(x' - x_1, y' - y_1, z', z_1)|^2}{\iint_{x,y} \int_{-\infty}^{0} |\mathbf{E_0}(x' - x_1, y' - y_1, z', z_1)|^2 dx' dy' dz'} dx' dy' dz'. \quad (9)$$

The 2D Fourier transform of (9) leads to the Fredholm integral equation for NST:

$$\varepsilon_1^{\text{eff}}(\kappa_x, \kappa_y, D) = \int_{-\infty}^{0} \varepsilon_1'(\kappa_x, \kappa_y, z') K(\kappa_x, \kappa_y, D, z') dz'. \quad (10)$$

It is easily seen that the kernel K in Eq. (10) is the same as the kernel K in Eq. (8) derived above for the passive temperature tomography. If a plane antenna is placed in the x-y plane at the altitude $z \geq 0$, the reference field for the x component of current's distribution over its aperture $\mathbf{j^p}(x, y, z) = j_x^p(x, y) \delta(z - z_1)$ is obtained from Eq. (1) as

$$\mathbf{E}_0(x - x_1, y - y_1, z, z_1) = -\frac{1}{2\omega} \int_{-\infty}^{\infty} \int_{-\infty}^{\infty} j_x^p(\kappa_x, \kappa_y) \frac{\exp\{i\kappa_x(x - x_1) + i\kappa_y(y - y_1) \pm i\sqrt{k^2 - \kappa_\perp^2} z \pm i\sqrt{k_0^2 - \kappa_\perp^2} z_1\}}{\sqrt{k_0^2 - \kappa_\perp^2}}$$

$$\times \{f_x^{E0}(\kappa_x, \kappa_y, \varepsilon_0)\vec{x}_0 + f_y^{E0}(\kappa_x, \kappa_y, \varepsilon_0)\vec{y}_0 + f_z^{E0}(\kappa_x, \kappa_y, \varepsilon_0)\vec{z}_0\} d\kappa_x d\kappa_y,$$

$$f_x^{E0} = \frac{1}{\kappa_\perp^2}[\kappa_x^2(k_0^2 - \kappa_\perp^2)T_{||} + \kappa_y^2 \kappa_0^2 T_\perp], \qquad f_y^{E0} = \frac{\kappa_x \kappa_y}{\kappa_\perp^2}[(k_0^2 - \kappa_\perp^2)T_{||} - k_0^2 T_\perp], \qquad f_z^{E0} = \mp \kappa_x \sqrt{k_0^2 - \kappa_\perp^2}\, T_{||}, \quad (11)$$

$k_0 = \omega/c$, $T_{||}$, $T_\perp$ are Fresnel coefficients, $j_x^P(\kappa_x, \kappa_y)$ is the lateral spectrum of the current. Using (11) for a homogeneous current distribution $j_x^p = $ const in the rectangle $|x - x_1| < L_x/2$, $|y - y_1| < L_y/2$ with the spectrum $j_x^p(\kappa_x, \kappa_y) = j_x \sin\kappa_x L_x \sin\kappa_y L_y / 4\pi^2 \kappa_x \kappa_y$, typical for

electrically small plane dipoles, the kernel $K(k_x, k_y, z)$ of (8) and (10) is obtained as the exact expression $K(k_x, k_y, z, L_x, L_y, z_1)$ that depends on sizes L_x, L_y of a plane antenna and on its height z_1 above the medium surface. These parameters and the frequency of measure-
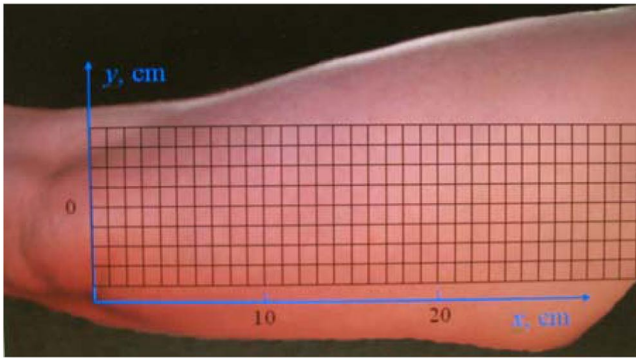

FIG. 1 (color online).   Scheme of microwave impedance scanning.

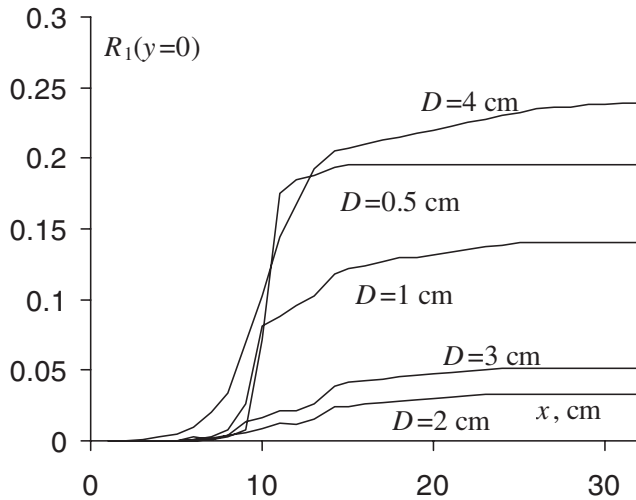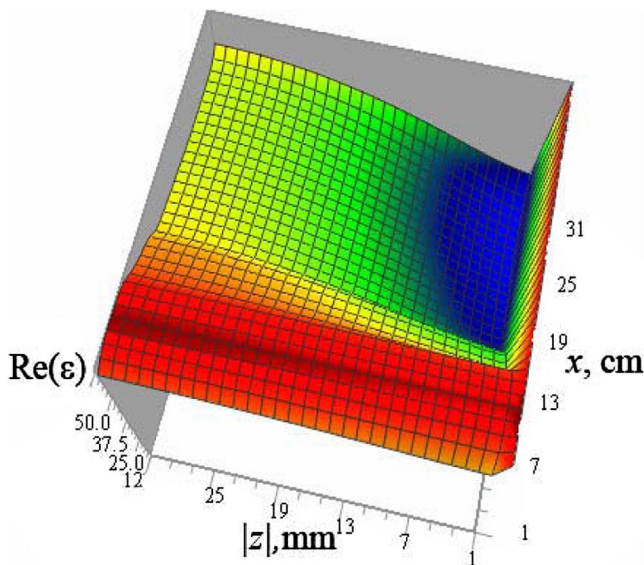FIG. 2 (color online).   Set of near-field resonant antennas.

FIG. 3.   Variations of the reflection coefficient.

ments ω can be used as the depth-of-formation parameter D in passive and active microwave NST.

Microwave NST of living tissues.—The region of the human hip surface shown in Fig. 1 has been scanned at the surface level ($z_1 = 0$) using near-field dipole resonant antennas (see Fig. 2) at the frequency 1.15 GHz. The total length of dipoles was used as D in (10); i.e. $D = L_x = L_y = 0.5$, 1, 2, 3, and 4 cm. The effective depth of the signal formation $d_{\mathrm{eff}}(D) = | \int_{-\infty}^{0} z \iint K(x, y, z, D) dx dy\, dz|$ is increased with D from 0.2 up to about 2 cm. The one-dimensional Fredholm integral equation of the first kind (10) is solved by Tikhonov's method, and the 2D inverse Fourier transform of the obtained profile of lateral spec-

trum components gives us the desired solution of this tomography problem. [We have operated within the standards of the Helsinki Declaration of the World Medical Associations. The applied (and monitored) power was lower than that of a cell phone signal and was judged to impose no measurable risk. The subject knew what was being done and was informed of the risk level and voluntarily agreed to participate in measurements and be exposed to the above-mentioned microwave signal.]

In Fig. 3 results of scanning of the reflection coefficient variations $R_1(x, y)$ at $y = 0$ along the x direction from the knee (the depth of the fat is increasing in this direction) are shown for all antennas in Fig. 2.

The tomography of the real part of permittivity $\varepsilon'(x, y, z)$ (sectional view $y = 0$) in living tissues in Fig. 4 is obtained with a subwavelength resolution (sizes of the tomogram are less than the wavelength $\lambda = 26.1$ cm). It is clearly seen from Fig. 4 that the hypodermic permittivity decreases sharply from the knee in the x direction from values typical for muscle and bone tissues, to the values typical for the fat. Results are in quite reasonable correspondence with the real structure of living tissues.

FIG. 4 (color online).   Tomography of $\varepsilon'(x, y, z)$ of living tissues.

[1] J. Radon, *Uber die Bestimmung von Funktionen durchihre Integralwerte Langs Ge wisser Mannigfaltigkiten* (Berlin Academy of Sciences, Leipzig, 1917).
[2] A. N. Tikhonov, V. Y. Arsenin, and A. A. Timonov, *Mathematical Problems of Computer Tomography* (Moscow Press, Nauka, 1987).
[3] P. S. Carney and J. C. Schotland, Appl. Phys. Lett. **77,** 2798 (2000).
[4] P. S. Carney, V. A. Markel, and J. C. Schotland, Phys. Rev. Lett. **86,** 5874 (2001).
[5] P. S. Carney and J. C. Schotland, J. Opt. A Pure Appl. Opt. **4,** S140 (2002).
[6] P. S. Carney and J. C. Schotland, J. Opt. Soc. Am. A **20,** 542 (2003).
[7] P. S. Carney, R. A. Frazin, S. I. Bozhevolnyi, V. S. Volkov, A. Boltasseva, and J. C. Schotland, Phys. Rev. Lett. **92,** 163903 (2004).
[8] P. S. Carney and J. C. Schotland, in *Inside Out: Inverse Problems,* edited by Gunther Uhlman (Cambridge University, Cambridge, 2003).
[9] K. P. Gaikovich, *Inverse Problems in Physical Diagnostics* (Nova Science, New York, 2004).
[10] K. P. Gaikovich, A. N. Reznik, V. L. Vaks, and N. V. Yurasova, Phys. Rev. Lett. **88,** 104302 (2002).
[11] O. J. F. Martin, C. Girard, and A. Dereux Phys. Rev. Lett. **74,** 526 (1995).
[12] A. N. Tikhonov and V. Y. Arsenin, *Solutions of Ill-Posed Problems* (John Wiley, New York, 1977).
[13] A. N. Reznik and N. V. Yurasova, J. Appl. Phys. **98,** 114701 (2005).